Title

Manipulate the Electronic and Magnetic States in NiCo2O4 Films through Electric-Field-Induced Protonation at Elevated Temperature

Journal

Advanced Materials, 31(16)

ISSN

0935-9648

Authors

Wang, Meng
Sui, Xuelei
Wang, Yujia
et al.

Publication Date

2019-04-01

DOI

10.1002/adma.201900458

Peer reviewed

Manipulate the Electronic and Magnetic States in $NiCo_2O_4$ Films through Electric-Field Induced Protonation at Elevated Temperature

Meng Wang, Xuelei Sui, Yujia Wang, Yung-Hsiang Juan, Yingjie Lyu, Huining Peng, Tongtong Huang, Shengchun Shen, Chenguang Guo, Jianbing Zhang, Zhuolu Li, Hao-Bo Li, Nianpeng Lu, Alpha T. N'Diaye, Elke Arenholz, Shuyun Zhou, Qing He, Ying-Hao Chu, Wenhui Duan and Pu Yu**

M. Wang, Dr. X. Sui, Y. Wang, Y. Lyu, H. Peng, T. Huang, J. Zhang, Z. Li, Dr. S. Shen, Dr C. Guo, Dr. H. -B. Li, Dr. N. Lu, Prof. S. Zhou, Prof. W. Duan, Prof. P. Yu
State Key Laboratory of Low Dimensional Quantum Physics and Department of Physics, Tsinghua University, Beijing 100084, China

Email: yupu@tsinghua.edu.cn and dwh@phys.tsinghua.edu.cn

Y. -H. Juan, Prof. Y. -H. Chu
Department of Materials Science and Engineering, National Chiao Tung University, Hsinchu 30010, Taiwan

Dr. A. T. N'Diaye, Dr. E. Arenholz
Advanced Light Source, Lawrence Berkeley National Laboratory, Berkeley, California 94720, USA.

Prof. Q. He
Department of Physics, Durham University, Durham DH13LE, United Kingdom.

Prof. W. Duan, Prof. P. Yu
Collaborative Innovation Center of Quantum Matter, Beijing 100084, China

Prof. P. Yu
RIKEN Center for Emergent Matter Science (CEMS), Wako 351-198, Japan

Keywords: spinel, ionic liquid gating, protonation, phase transformation

Abstract: Ionic liquid gating (ILG) induced proton evolution emerges as a novel strategy to realize electron doping and manipulate the electronic and magnetic ground states in complex oxides. While the study of a wide range of systems (e.g. $SrCoO_{2.5}$, VO_2, WO_3, etc.) has demonstrated important opportunity to incorporate protons through ILG, the protonation remains a big challenge for many others. Besides, the

mechanism of proton intercalation from the ionic liquid/solid interface to whole film

has not been revealed yet. Here, with a model system of inverse spinel NiCo2O4, we

show that the increase of system temperature during ILG forms a single but effective

method to efficiently affiliate the protonation. Moreover, we show the ILG induces a

novel phase transformation in NiCo2O4 from ferrimagnetic metallic into

antiferromagnetic insulating with protonation at the elevated temperature. This study

brings the environmental temperature as an efficient tuning knob to manipulate the

ILG induced ionic evolution.

Ionic liquid gating (ILG) has attracted wide range research attention in the last two

decades [1], leading to the discovery of a plethora of exotic phenomena, such as

metal-insulator transition (MIT) [2-4], magnetism [5] and superconductivity [6-9] in

various material systems. In the conventional ILG, the tunability is mainly dominated

by an electrostatic effect occurred at the liquid/solid interface [2-9], while any

electrochemical reaction during the gating is carefully avoided [1,10]. However, it has

been demonstrated recently that the residual water would exist ubiquitously within the

ionic liquid (IL) when experiments performed in the air [11-14]. The water molecular

would facilitate the electrochemical reaction through electrolysis into H^+ and O^{2-} ions,

which would then be inserted into materials depending on the polarity of the gating

bias [11-17] (as shown in **Figure 1a**). Clearly the electrochemical reaction related

modulation is a bulk effect, and therefore its associated charge modulation should not

be confined by the two dimensional limit as the conventional ILG, which is about

$10^{15}/cm^2$ at the sample surface [2-8]. Along these studies, the H^+ (proton) ion, the

smallest and lightest ion, emerges as an ideal candidate to incorporate into materials for the manipulation of band filling via charge neutrality induced electron doping with positively charged proton [13,18]. Besides, protonated materials have tremendous application potential in hydrogen storage [18] and fuel cells [19-22]. So the study of ILG induced protonation is significant for both fundamental physics (realizing electron doping and phase control) and industry application (discovering new protonated functional materials). It is important to note that although the ILG induced protonation has been demonstrated in a few model systems, such as VO2[11], SrCoO [12], and WO [13,14], the underlying mechanism of the protonation process evolution is not resolved yet.

NiCo2O4 (NCO) is an inverse spinel structure composed of the face-centered cubic lattice with alternative stacking of oxygen octahedra (NiO6, CoO6) as well as tetrahedra (CoO4) [23], as shown in **Figure 1b**. Due to its application potential in spintronics [23], catalysis [24-27], batteries [28], photodetectors [29], etc., NCO attracts increasing research interests. It has been demonstrated that the growth temperature of

NCO can largely modulate its chemical stoichiometry and therefore manipulate the corresponding electronic and magnetic ground states [23,30]. When fabricated at a temperature below 400℃, NCO thin film shows an exotic ferrimagnetic metallic state, while at higher growth temperature, the material changes into an insulating state. This interesting transition can be attributed to the intermixing of the Ni and Co ions for sample grown at higher temperature, which would lead to the reduction of the Ni valence state, and therefore change the band structure as well as magnetism [23,30].

Motivated by its readily tuned valence states for both Ni and Co ions in NCO as well its strongly correlated magnetic and electronic properties, we consider NCO as a nice candidate to explore the mechanism of ILG induced protonation, and realize novel electronic and magnetic ground states with different functionalities.

In this work, we demonstrate that the elevated system temperature during ILG can dramatically enhance the protonated phase transformation process in NCO, and generate a new protonated NCO phase which however cannot be obtained through the conventional ILG performed at room temperature. Combining hydrogen forward scattering and soft X-ray absorption spectroscopy measurements, we show clear experimental evidence that the protonation causes the formation of a novel H2NiCo2O4 (HNCO) structure, leading to distinct electron doping into the pristine sample. As a consequence, the material changes from a ferrimagnetic metallic into an antiferromagnetic insulating state. This study takes the understanding of ILG induced protonation process a step further, provides a generic strategy (i.e. increasing temperature) to boost this effect in extended material systems, as well as reveals a

novel protonated spinel structure.

NCO thin films were grown on MgAl2O4 (004) substrates by pulsed laser deposition

at a substrate temperature of 350℃ (see **Experimental Section** for details) to obtain

the ferrimagnetic metallic phase. The XRD 2θ - ω scan in **Figure 1c** indicates a high

quality epitaxial single-crystalline nature of the thin films, which is also consistent

with previous reports [23,30]. We carried out ILG measurements with the experimental

configuration shown in **Figure 1a**, with the as-received DEME-TFSI ionic liquid (with the H2O concentration of ~390 ppm in mass [12]) as the electrolyte. With increasing the gate voltage to 4.5V at room temperature, the NCO thin film shows a large structural expansion with the emergence of a new diffraction peak at ~41.50º, but a notable peak persists at the original position (around 44.20º) even after extended gating for 10 hours (**Figure 1c**). We speculate that this is related to the high proton insertion barrier and poor proton diffusion coefficient, resulting in the electrochemical reaction only confined at the NCO surface. To facilitate the protonation process during the ILG, we increased slightly the environment temperature to 100℃, and then the whole film transforms into the new phase at 4.5 V (**Figure 1c**). Besides, the newly developed structure remains unchanged even after reducing the gating voltage to zero and can be stable in air at room/ambient temperature for weeks, indicating that the phase transformation is nonvolatile. In contrast to SrCoO2.5, in which the phase transformation is reversibly controllable by electric field [12], the new phase remains stable even with the application of an opposite negative gating voltage. Nevertheless,

the reverse phase transformation can be achieved through thermal annealing in air as shown in **Figure 1d**. We note that despite of the induced large chemical expansion (about 6.08%) along the out-of-plane direction, the in-plane lattice parameter is strongly constrained by the substrate (**Figure 1e)**, indicating that the film remains coherently strained through the ILG process. A hydrogen forward scattering (HFS) measurements was also performed on the new phase to probe directly the hydrogen concentration (see **Experimental Section** and **Figure 1f**), which provides a

quantitative estimate of the hydrogen area density as 9.64×10^{16} atoms / cm^2. Knowing the film thickness (~37 nm) and lattice constants, we can then estimate the H+/(NiCo2O4) ratio in the new phase as ~1.86.

To achieve a deep understanding of the difference of the ILG induced protonation at different gating temperatures, we carried out the cyclic voltammetry measurements with the comparison of *in-situ* XRD studies during the ionic liquid gating (**Figure 2**).

At the room temperature, the cyclic voltammograms (**Figure 2a)** show a clear peak at ~1.5 V (point A), which should be attributed to the electrolysis process of the water content. We note that similar critical voltages were also observed at the model system of SrCoO2.5 and WO3 [12,13], which are all slightly larger than the theoretical value of ~1.23 V at room temperature due to the presence of the over potential. However, different from the SrCoO2.5, in which the protonation occurs at about 1.5 V, the NiCo2O4 phase remains unchanged through the ILG as evidenced by the *in-situ* XRD measurements at the same voltage region (**Figure 2b**). Since the proton is positively charged, it would accumulate at the sample surface with the application of positive

biased voltage to form the so-called double layer [1,13]. Therefore, the application of larger bias above 1.5 V would increase the proton content at the sample surface and consequently lead to the enhancement of the chemical potential for proton at the surface. When the chemical potential for proton at the liquid/material interface is larger enough to overcome the barrier for proton intercalation, the proton would be inserted into the top layer of the material and lead to a phase transition only at the very top layer, as evidenced by a clear peak at about 3.5 V (peak B) in the

voltammograms (**Figure 2a**), as well as the emergence of a new diffraction peak in the *in-situ* XRD results (**Figure 2b**). However, the majority region of the thin film remains unchanged even with the gating voltage up to 4.5 V (also illustrated in **Supplementary Figure 1**).

We note that since NiCo2O4 is metallic, and the gate voltage would generate no electric-field inside due to the screening effect. Therefore, the main driving force for the proton transfer would be the diffusion process due to the presence of the proton concentration gradient. However, in contrast with that of SrCoO2.5 and WO3 [12,13], this process is strongly suppressed in NiCo2O4 likely due to its negligible proton diffusion coefficient. With this discussion, one would expect that the elevated gating temperature can naturally enhance the proton diffusion coefficient ($D(T)$) due to its temperature (T) dependence as $D(T)=D_o\,exp\,(-E_a/kBT)$ [19], where E_a is the activation energy and kB is the Boltzmann constant. When ILG were performed at 100℃, as shown in **Figure 2c**, the water electrolysis and proton intercalation processes were also observed while with clearly suppressed critical voltages (labelled as A’ and B’).

More interestingly, we also observed a new peak in the cyclic voltammograms at ~ 4.0 V (labelled as C’), indicating a new proton exchange process. At the same voltage region, we observed a clear structural transformation from the NiCo2O4 to the protonated phase with the totally disappearance of its corresponding diffraction peak for the NiCo2O4 phase (**Figure 2d**).

With these new experimental observation, we can assign the ILG induced protonation

process into three subsequent steps, electrolysis, intercalation and diffusion

(**Supplementary Figure 1**). While the first two steps are correlated with both the

applied gating voltage and environmental temperature, the last step is mainly

determined by the intrinsic diffusion coefficient of the materials, therefore only

influenced strongly by the environmental temperature [18,19]. Accordingly, the change

of the gating temperature forms a unique tuning strategy to assist the ILG induced

structural transformations. To the best of our knowledge, this work presents the first

experiment with ILG performed at elevated temperature, while conventionally the

ILG is performed usually at room temperature and below [1-15]. Along this vein, this

work forms a substantial advance of this powerful ionic liquid gating method, and

generates a new strategy to achieve controllable structural phase transformation with

the gating temperature as an efficient tuning knob. Indeed, with this new strategy, the

protonation process can be further enhanced in the model system of $SrCoO_{2.5}$ [12] (as

shown in **Supplementary Figure 2**), in which the protonation duration is suppressed

from 70 min (30ºC) to only about 12 min (100ºC). Moreover, the proton concentration

in HxSrCoO2.5 is likely further enhanced for the sample gated at elevated temperature,

as its corresponding diffraction peak shifts from 44.0º (30ºC) further to 43.6º (100ºC).

Following the discussion of the improved ILG method, we further studied the

electronic and magnetic properties of the protonated NCO phase. First, to probe the

valence states of the corresponding transition metal elements on both pristine and

protonated NCO samples, we performed the soft X-ray absorption spectroscopy (XAS)

measurements (see **Experimental Section**). The XAS results on the pristine NCO

sample shows a mixed valence state of 2^+ and 3^+ for both Ni and Co ions (**Figure 3a, b**), which is consistent with the previous study [23]. On the other hand, the measurements on the protonated samples show a distinct shift of the absorption peaks towards lower energy as compared with those from the pristine sample. Using NiO and CoO as references [23], the valence state for both Ni and Co can be assigned as 2^+.

Since the bulk-sensitive total luminescence yield (TLY) mode was employed during the XAS measurements, one can then readily conclude that the valence modulation (i.e. chemical evolution) occurs throughout the entire film. Moreover, we also compared the K-edges of oxygen for these two phases. As shown in **Figure 3c**, the pre-peak near 529 eV in NCO is totally suppressed in the protonated phase, which is consistent with the experimental results observed in protonated SrCoO2.5, suggesting the suppression of O-2p and Ni (Co)-3d hybridization [12]. Considering that both Ni and Co ions assume the reduced 2^+ valence state and the large amount of hydrogen atoms distribute within the protonated phase, we can conclude that the protonation during ILG plays an essential role for the observed phase transformation. Accordingly,

we can assign the stoichiometry of the protonated phase as $H_2NiCo_2O_4$.

Knowing the dramatic change of the valence states and crystalline structure during the phase transformation, one might naturally expect the emergence of a novel magnetic and electronic state in the protonated phase. To reveal the magnetic properties, we first measured the hysteresis (*M*-*H*) loops and the temperature dependent magnetization (*M*-*T*) (see **Experimental Section**) for both pristine and protonated samples. As shown in **Figure 4a**, the pristine NCO shows a typical ferromagnetic

loop at 20 K with a saturation magnetization of about 240 emu / cm^3 (corresponding to 1.8 μ_B per formula unit cell), while the corresponding hysteresis loop for the protonated phase shows strongly reduced magnetization (<20 emu /cm^3). Furthermore, although the temperature dependent magnetization measurement (as shown in **Figure 4b**) shows a clear ferrimagnetic transition for the pristine sample with the transition temperature around 260 K, there is no distinct magnetic transition measured across the whole measured temperature region for the protonated one. To provide further insights for the observed distinct magnetic state, we carried out soft X-ray magnetic circular dichroism (XMCD) measurements (see **Experimental Section**) on both Ni (**Figure 4c**) and Co (**Figure 4d**) *L*-edges, which can provide element-specific information for the magnetic states. In the pristine sample, the Ni and Co ions show an anti-parallel coupling, in agreement with the previous reports in this inverse spinel structure and indicating a ferrimagnetic ground state [23,30,31]. By contrast, the XMCD measurements on the protonated sample show no spin-polarization for both Ni and Co ions. Therefore, we can deduce that the protonated phase forms an antiferromagnetic

state, and the measured small magnetization (**Figure 4a)** can be attributed to the small canting moment [32].

We further investigated the electronic state of the protonated phase through the optical transmittance and transport measurements (see **Experimental Section**). The insert in **Figure 4e** shows a direct comparison of the optical photographs for pristine and protonated NCO films as well as the referenced bare MgAl2O4 substrate. It is clear that, through the protonation, the NCO film changes from opaque into transparent,

indicating the modulation of the optical transparency through protonation. As shown in **Figure 4e**, the protonated sample shows strongly enhanced optical transmittance throughout the measured wavelength region as comparing with the pristine one.

Similarly, the transport measurements reveal that the pristine NCO shows a clear metallic temperature dependent behavior (**Figure 4f**), which is consistent with previous reports [23,30]. While on the other hand, the protonated sample shows an insulating behavior with more than five orders of magnitude enhancement of resistivity at the room temperature. With these experimental results, we can readily conclude that NCO thin film undergoes a metallic to insulating transformation through the ILG induced protonation. More importantly, a simple thermal annealing of the protonated sample at 400ºC in air can nicely reverse it back into the pristine state with the recovery of the corresponding optical, magnetic and electronic properties (**Supplementary Figure 3**).

To obtain theoretical insights for the electronic and magnetic ground states of the protonated NCO sample, we performed first-principles calculations [33-38] (see

Experimental Section). We first calculated the atomic structure for the pristine phase with the in-plane lattice constant fixed with that of the substrate. The calculated projected density of state (PDOS) (as shown in **Figure 5c**) reveals a ferrimagnetic metallic state. From the PDOS, the calculated magnetizations are estimated as ~ -0.9 **μ_B** and ~ +2.8 μ_B for Ni and Co ions respectively. Therefore, the total magnetization can be estimated as 1.9 μ_B per chemical formula, which is consistent with both our experiment results and the previous calculations [31].

To mimic the protonation process, we randomly inserted two H^+ ions into the crystalline lattice and then fully relaxed the atom positions to achieve the corresponding energetically favorable structure. As shown in **Figure 5a and b**, in the lowest energy structure for the protonated phase, the H^+ ions tend to form bonds with the oxygen ions, leading to a large lattice expansion along the (001) direction. The calculated *c* lattice constant is 8.67Å for the protonated H2NiCo2O4 phase, in excellent agreement with our experimental result of 8.69Å. The calculated PDOS of the protonated phase shows the development of a well-defined band gap (about 0.5 eV) (**Figure 5d**), nicely consistent with the indirect band gap obtained from the optical transmittance spectra (**Supplementary Figure 4**). Furthermore, the PDOS for Ni ions (at the octahedra) shows a quenched spin-polarization, which suggests that the Ni ions do not contribute to the magnetism. On the other hand, the PDOS of Co ions at the octahedra and tetrahedra sites contributes -2.6 μ_B and 2.5 μ_B respectively, indicating an intrinsic antiferromagnetic spin alignment for Co ions located at different sites.

These calculated results are consistent with our experimental results, suggesting that

the protonated phase is an antiferromagnetic insulator.

To summarize, within this study, we have obtained a further understanding of the underlying mechanism of ILG induced protonation and demonstrate that the gating temperature forms a tuning knob to boost effectively the protonation to realize the electron doping and enrich the phase diagram. The associated electron doping into protonated NCO leads to a distinct transformation of the electronic and magnetic ground state from ferrimagnetic metallic into antiferromagnetic insulating, and the

novel $H_2NiCo_2O_4$ phase would expand the knowledge of spinel systems for wide range of applications. Finally, this simple but effective method could be readily extended to a large group of materials, providing an important strategy to manipulate the electronic and magnetic ground states with desirable material functionalities.

Experimental Section

***Thin Film Fabrication*:** $NiCo_2O_4$ thin films were grown on $MgAl_2O_4$ (001) substrates by a home-designed pulsed laser deposition system. The deposited temperature was controlled to be 350 oC with a O_2 pressure of 20 Pa. The energy density of pulsed laser (wavelength 248 nm) was around 1.2 J/cm^2 and the repetition frequency was 5 Hz.

After the deposition, the samples were cooled down to room temperature in 0.5 bar of O_2 with the cooling rate of 5 oC per minute.

Ionic Liquid Gating and X-ray Diffraction Measurements: Films were contacted with Pt wire by colloidal silver pasted at the edges and then placed in a quartz bowl filled with ionic liquid. The gating voltage was applied between the sample and the gate electrode, which is a screwed Pt wire. The bowl was then fixed on top a thermal heater, in which the temperatures can be digitally controlled. The X-ray diffraction (XRD) measurements were carried out with a high-resolution diffractometer (Smartlab, Rigaku) using monochromatic Cu $K_{\alpha 1}$ radiation (λ = 1.5406 Å).

Hydrogen Forward Scattering (HFS) Measurement: HFS measurements were

performed in a Rutherford Backscattering Facility at EAG Laboratory. During HFS experiment, a detector was placed 30 ^{o} from the forward trajectory of the incident He^{++} ion beam and the sample was rotated so that the incident beam strikes the surfaces 75^{o} from normal. Spectra were fit by applying a theoretical model and iteratively adjusting the hydrogen concentrations and film thickness until good agreement was achieved between the theoretical and the experimental spectra. Hydrogen concentrations were determined by comparing the hydrogen counts with that obtained

from reference samples after normalizing with the stopping powers of the different materials. Here a hydrogen implanted silicon sample (with a hydrogen areal density of 1.6×10^{17} atoms per cm) was used as the reference. The protonated sample with a dimension of 100 mm^2 and a thickness of 45 nm was prepared. An Ar-ion etching process was carried out with about 8 nm surface etched away to clean organic pollution before the HFS measurement.

X-ray Absorption Spectroscopy (XAS) Measurements: XAS at cobalt and nickel *L*-edges were measured by bulk-sensitive total luminescence yield (TLY) mode and the oxygen *K*-edges were measured in total electron yield (TEY) mode at Beamlines 4.0.2 and 6.3.1 of Advanced Light Source and Beamline 25 of Spring 8 Synchrotron Radiation Facility. The X-ray magnetic circular dichroism (XMCD) studies were carried out at beamline 4.0.2 of Advanced Light Source, with 90% circularly polarized X-rays incident along the film normal. During the measurements, the temperature was kept at 20 K with a magnetic field of ±4.0 T applied along the beam incident direction.

Magnetization, Optical Transmittance and Transport

Measurements: The magnetic properties of all samples were measured with a Magnetic Property Measurement System (MPMS, Quantum Design). The magnetic-field was applied along the in-plane direction. Optical transmittance spectra were measured in air at room temperature with a spectrophotometer (Cary 5000 UV-Vis-NIR, Agilent and Excalibur 3100, Varian). Electrical resistance was measured by a Quantum Design DynaCool system through four-probe electrical contact geometry to eliminate the influence of

contact resistance.

Density Functional Theory (DFT) Calculations: All calculations are conducted within the framework of density functional theory (DFT) [33] as implemented in the Vienna *ab initio* simulation package (VASP) [34]. The core electron potentials are described by the projector augmented-wave (PAW) potential [35]. The exchange correlation interactions are described by the generalized gradient approximation (GGA) [36] in the form of Perdew-Burke-Ernzerhof (PBE). Moreover, GGA+*U* [37] method is employed to treat the strong on-site Coulomb interaction of Co and Ni atoms. To simulate the distinct magnetic interactions among the ions for pristine and protonated samples, different *U* values were selected for each phase [38]. The *U* values chosen for Ni atom are 3.5 and 6.5 eV, for Co atom 5.5 and 6.5 eV for NiCo2O4 and H2NiCo2O4, respectively. After the protonation process, the charge density around oxygen and magnetic ions are dramatically modified, therefore the exchange constants *J* for inter and intra magnetic ions as well as the Coulomb repulsion energy are also strongly affected. For simplicity, we neglected the intermixing of the Ni and

Co ions in the calculation and considered the case of NCO with perfect inverse spinel

structure. During the calculation, the crystalline structures were fully relaxed until the

remaining force acting on each atom is no more than 0.01 eV/Å. In order to yield

well-converged total energies, the plane wave basis with a kinetic energy cutoff of

400 eV was used.

Supporting Information: Supporting Information is available from the Wiley Online Library or from the author.

Acknowledgements: M. W., X. S. and Y. W. contributed equally to this work. This study was financially supported by the Basic Science Center program of NSFC (grant No. 51788104); NSFC (grants 2015CB921700 and 2016YFA0301004); the National Natural Science Foundation of China (grant No. 51872155); and the Beijing Advanced Innovation Center for Future Chip (ICFC). The Advanced Light Source is supported by the US Department of Energy under contract no. DE-AC02-05CH11231.

References

[1] S. Z. Bisri, S. Shimizu, M. Nakano, Y. Iwasa, *Adv. Mater.* **2017**, *29*, 1607054.

[2] A. S. Dhoot, C. Israel, X. Moya, N. D. Mathur, R. H. Friend, *Phys. Rev. Lett*. **2009**, *102*, 136402.

[3] R. Scherwitzl, P. Zubko, I. G. Lezama, S. Ono, A. F. Morpurgo, G. Catalan, J. M. Triscone, *Adv. Mater*. **2010**, *22*, 5517.

[4] M. Nakano, K. Shibuya, D. Okuyama, T. Hatano, S. Ono, M. Kawasaki, Y. Iwasa, Y. Tokura, *Nature* **2012**, *487*, 459.

2011, *472*,

[5] Y. Yamada, K. Ueno, T. Fukumura, H. T. Yuan, H. Shimotani, Y. Iwasa, L. Gu, S. Tsukimoto, Y. Ikuhara, M. Kawasaki, *Science* **2011**, *332*, 1065.

[6] K. Ueno, S. Nakamura, H. Shimotani, A. Ohtomo, N. Kimura, T. Nojima, H. Aoki, Y. Iwasa, M. Kawasaki, *Nat. Mater*. **2008** ,*7* , 855.

[7] A. T. Bollinger, G. Dubuis, J.Yoon, D. Pavuna, J. Misewich, I. Božović, *Nature* **2011**, *472*,

[8] J. T. Ye, Y. J. Zhang, R. Akashi, M. S. Bahramy, R. Arita, Y. Iwasa, *Science* **2012**, *338*, 1193.

[9] B. Lei, J. H. Cui, Z. J. Xiang, C. Shang, N. Z. Wang, G. J. Ye, X. G. Luo, T. Wu, Z. Sun, X. H. Chen, *Phys. Rev. Lett*. **2016**, *116*, 077002.

[10] J. Jeong, N. Aetukuri, T. Graf, T. D. Schladt, M. G Samant, S. S. P. Parkin, *Science* **2013**, *339*, 1402.

[11] K. Shibuya, A. Sawa, *Adv. Electron. Mater.* **2016**, *2*, 1500131.

[12] N. Lu, P. Zhang, Q. Zhang, R. Qiao, Q. He, H. Li, Y. Wang, J. Guo, D. Zhang, Z. Duan, Z. Li, M. Wang, S. Yang, M. Yan, E. Arenholz, S. Zhou, W. Yang, L. Gu, C. W. Nan, J. Wu, Y. Tokura, P. Yu, *Nature* **2017**, *546, 124*.

[13] M. Wang, S. Shen, J. Ni, N. Lu, Z. Li, H. Li, S. Yang, T. Chen, J. Guo, Y. Wang, H. Xiang, P. Yu, *Adv. Mater.* **2017**, *46*, 1703628.

[14] X. Leng, J. Pereiro, J. Strle, G. Dubuis, A. T. Bollinger, A. Gozar, J. Wu, N. Litombe, C. Panagopoulos, D. Pavuna, I. Božović, *npj Quantum Materials*, **2017**, *2:35*, 1.

[15] Y. Cui, G. Zhang, H. Li, H. Lin, X. Zhu, H. -H. Wen, G. Wang, J. Sun, M. Ma, Y. Li, D. Gong, T. Xie, Y. Gu, S. Li, H. Luo, P. Yu, W. Yu, *Science Bulletin*, **2018**, *63*, 11.

[16] C. S. Yang, D. S. Shang, N. Liu, G. Shi, X. Shen, R. C. Yu, Y. Q. Li, Y. Sun, *Adv. Mater.* **2017**, *29*, 1700906.

[17] J. -T. Yang, C. Ge, J. -Y. Du, H. -Y. Huang, M. He, C. Wang, H. -B. Lu, G. -Z. Yang, K. -J. Jin, *Adv. Mater.* **2018**, 201801548.

[18] H. Yoon, M. Choi, T. -W. Lim, H. Kwon, K. Ihm, J. K. Kim, S. -Y. Choi, J. Son,

Nat. Mater. **2016**, *15*, 1113.

[19] Y. Zhou, X. Guan, H. Zhou, K. Ramadoss, S. Adam, H. Liu, S. Lee, J. Shi, M. Tsuchiya, D. D. Fong, S. Ramanathan, *Nature* **2016**, *534*, 231.

[20] H. G. Bohn, T. Schober, *J. Am. Ceram. Soc*. **2000**, *83*, 768.

[21] L. Yang, S. Wang, K. Blinn, M. Liu, Z. Liu, Z. Cheng, M. Liu, *Science* **2009**, *326*, 126.

[22] D. Pergoles, E. Fabbri, A. D'Epifanio, E. D. Bartolomeo, A. Tebano, S. Sanna, S. Licoccia, G. Balestrino, E. Traversa, *Nat. Mater.* **2010**, *9*, 846.

[23] Y. Bitla, Y. -Y. Chin, J. -C. Lin, C. N. Van, R. Liu, Y. Zhu, H. -J. Liu, Q. Zhan, H. -J. Lin, C. -T. Chen, Y. -H. Chu, Q. He, *Scientific Reports* **2015**, *5:15201*,1.

[24] J. Zhu, Q. Gao, *Microporous Mesoporous Mater*. **2009**, *124*, 144.

[25] M. U. A. Prathap, R. Srivastava, *Nano Energy* **2013**, *2*, 1046.

[26] C. Davidson, G. Kissel, S. Srinivasan, *J. Electroanal. Chem.* **1982**, *132*, 129.

[27] Y. Li, P. Hasin, Y. Wu, *Adv. Mater*. **2010**, *22*, 1926.

[28] Y. Zeng, Z. Lai, Y. Han, H. Zhang, S. Xie, X. Lu, *Adv. Mater*. **2018**, *30*, 1802396.

[29] L. Hu, L. Wu, M. Liao, X. Fang, *Adv. Mater*. **2011**, *23*, 1988.

[30] P. Silwal, L. Miao, I. Stern, X. Zhou, J. Hu, D. H. Kim, *Appl. Phys. Lett.* **2012**, *100*, 032102.

[31] X. Shi, S. L. Bernasek, A. Selloni, *J. Phys. Chem. C* **2016**, 120 14892.

[32] J. -H. Lee, Y. K. Jeong, J. H. Park, M. -A. Oak, H. M. Jang, J. Y. Son, J. F. Scott, *Phys. Rev. Lett*. **2011**, *107*, 117201.

[33] W. Kohn, L. J. Sham, *Phys. Rev.* **1965**, *140*, A1133.

[34] G. Kresse, J. Furthmüller, *Comput. Mater. Sci.* **1996**, *6*, 15.

[35] P. E. Blöchl, *Phys. Rev. B* **1994**, *50*, 17953.

[36] J. P. Perdew, K. Burke, M. Ernzerhof, *Phys. Rev. Lett.* **1996**, *77*, 3865.

[37] V. I. Anisimov, F. Aryasetiawan, A. I. Lichtenstein, *J. Phys.: Condens. Matter* **1997**, *9*, 767.

[38] P. W. Anderson, *Phys. Rev.* **1950**, *79*, 350.

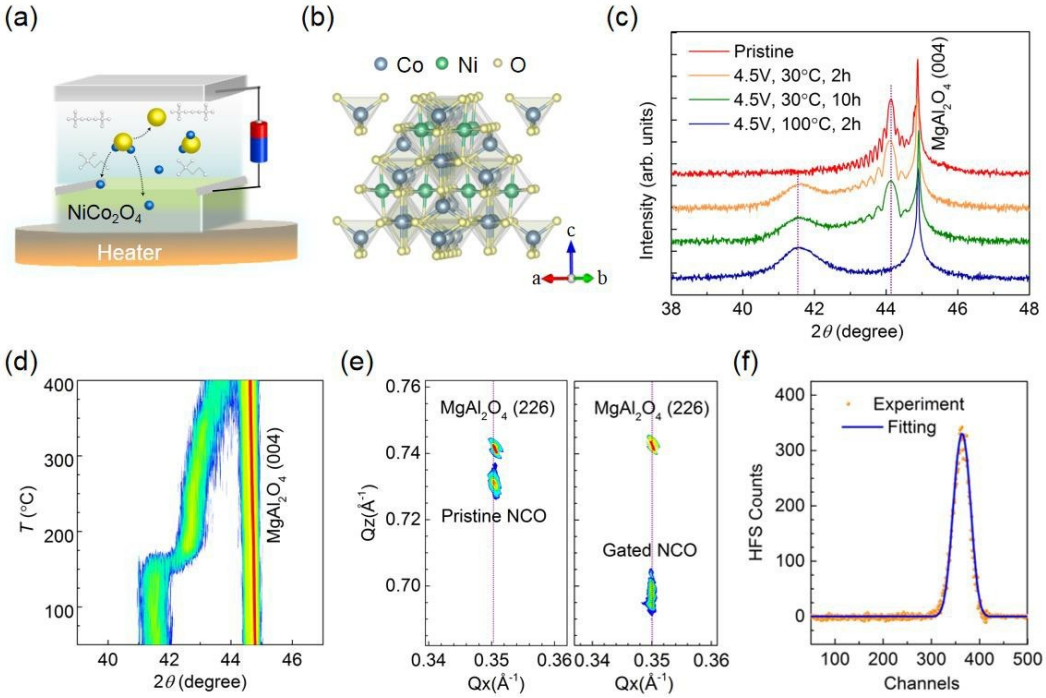

Figure 1. **Protonation induced structural phase transformation in NiCo2O4 films through ILG. a**) Schematic illustration of the experimental setup for the ionic liquid gating at elevated temperatures. **b**) Illustration of the crystalline structure of the inverse spinel NiCo2O4. In ideal inverse spinel NiCo2O4, the tetrahedra are all occupied by Co ions, while the octahedra are occupied by Ni and Co ions equally. **c**) Typical 2θ-ω scans of the pristine and gated NiCo2O4 films grown on MgAl2O4 (004) substrates. **d**) Temperature dependent 2θ-ω scans for a gated phase measured during

annealing in air. The curves were obtained at every 25ºC interval, with 5 minutes’ dwell time before each scan. **e**) Reciprocal space mapping (RSM) results of the pristine (left) and gated (right) samples measured around the $MgAl_2O_4$ (226) diffraction peak. **f**) Characterization of the hydrogen concentration in the gated $NiCo_2O_4$ film by HFS measurement.

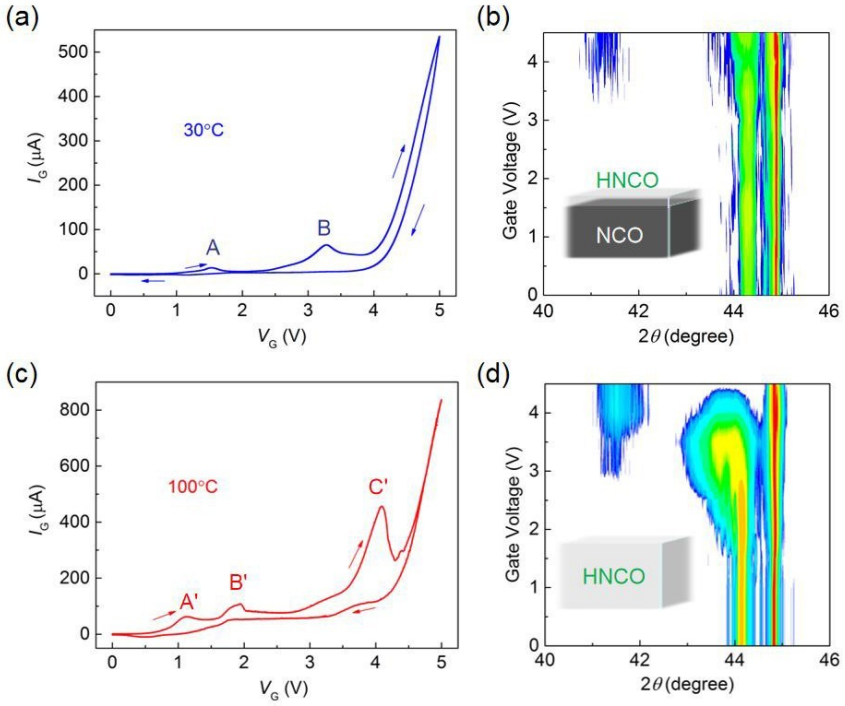

Figure 2. **Comparison of the proton evolution process in IL/NiCo2O4 system at**

different temperatures. Gate current (I_G) versus gate voltage (V_G) curves measured

at **a**) 30ºC and **c**) 100ºC. The voltage increased or decreased with a speed of 5 mV/s.

In-situ 2*θ*-*ω* scans of a NiCo2O4 film with gradual increasing gate voltage at **b**) 30ºC

and **d**) 100ºC. The curves were obtained at every 0.5 V interval, with 25 minutes'

dwell time before each scan. The insets illustrate the protonated region of the sample,

i.e. only top surface at 30ºC and whole film at 100ºC with V_G ≅ 4.5 V. All the measurements were carried out with the identical Pt electrodes and NCO films (4mm×5mm, and thickness = 45nm).

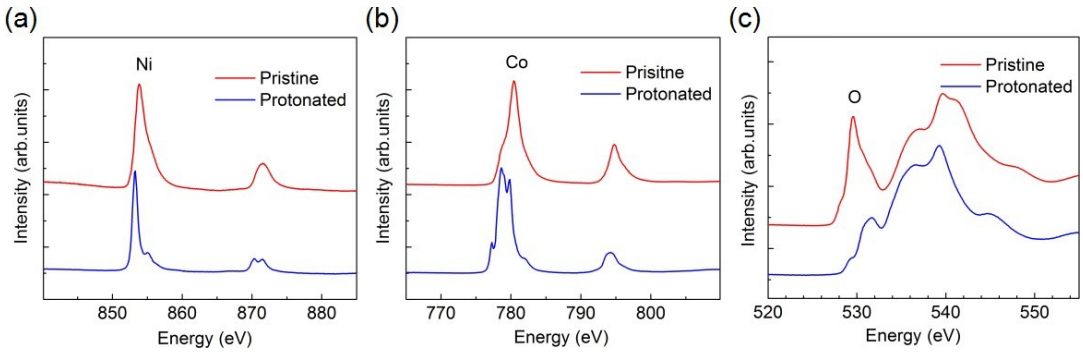

Figure 3. **Evolution of the valence states of $NiCo_2O_4$ with the ILG induced protonation.** Comparison of the X-ray absorption spectra at **a**) nickel *L*-edges, **b)** cobalt *L*-edges, and **c**) oxygen *K*-edges for the pristine (red) and protonated (blue) phases. The shifts of the peak positions and changes in line shape for both nickel and cobalt *L*-edges (toward lower energy) between the pristine and protonated phases suggest the reduced valence states through protonation. The oxygen *K*-edge spectra (around 529 eV) show distinct difference between these two phases, indicating the suppression of hybridization between Oxygen-2p orbital and the transition metal 3d orbital through protonation.

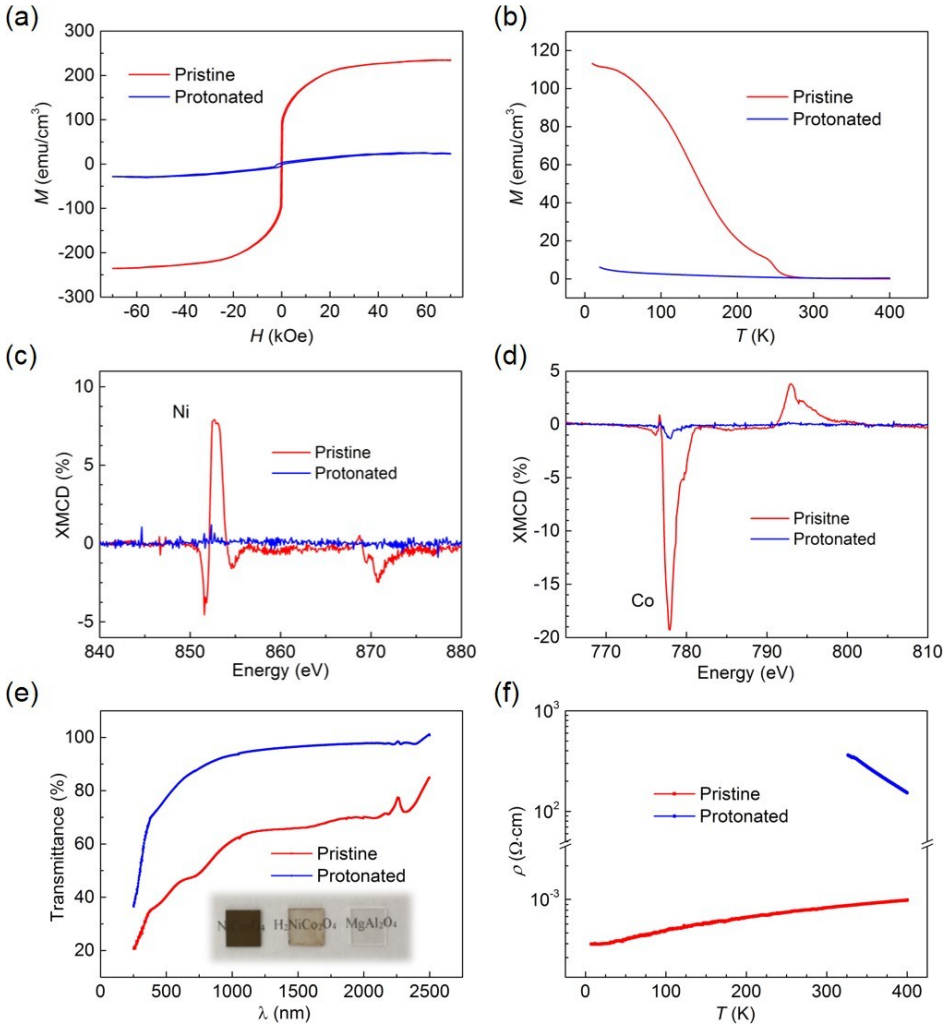

Figure 4. **Magnetic, optical and electronic properties in pristine and protonated NiCo2O4 films. a**) Comparison of the magnetic hysteresis loops for protonated and pristine phases, measured at 20 K with the magnetic field applied along the in-plane direction. **b**) Temperature dependent magnetization for these two phases. The data were obtained during the warming cycle with a magnetic field of 0.1 T. *X*-ray magnetic circular dichroism (XMCD) spectra at **c**) nickel and **d**) cobalt *L*-edges. The data were taken at 20 K with the magnetic field ±4 T applied along the incident

direction of the light, which is normal to the film plane. We note that the NCO is a soft magnetic material with small coercive and saturated magnetic fields. Therefore, the different measurement geometries between hysteresis loop and XMCD measurements should not influence the main conclusion. **e**) Optical transmittance spectra for the pristine and protonated films. In the protonation phase, the

transparency is dramatically enhanced among the whole spectral region. The inset shows comparison of the optical photographs for a 50nm $NiCo_2O_4$ thin films (left), the protonated $H_2NiCo_2O_4$ (middle) as well as a bare $MgAl_2O_4$ substrate (right). **f**) Temperature dependent resistivity for these two phases. The pristine sample shows a typical fermi liquid behavior, while the resistance of the protonated sample shows more than five orders of magnitude enhancement at the room temperature, and then are out of the measurement limit for the employed experimental setup at lower temperatures.

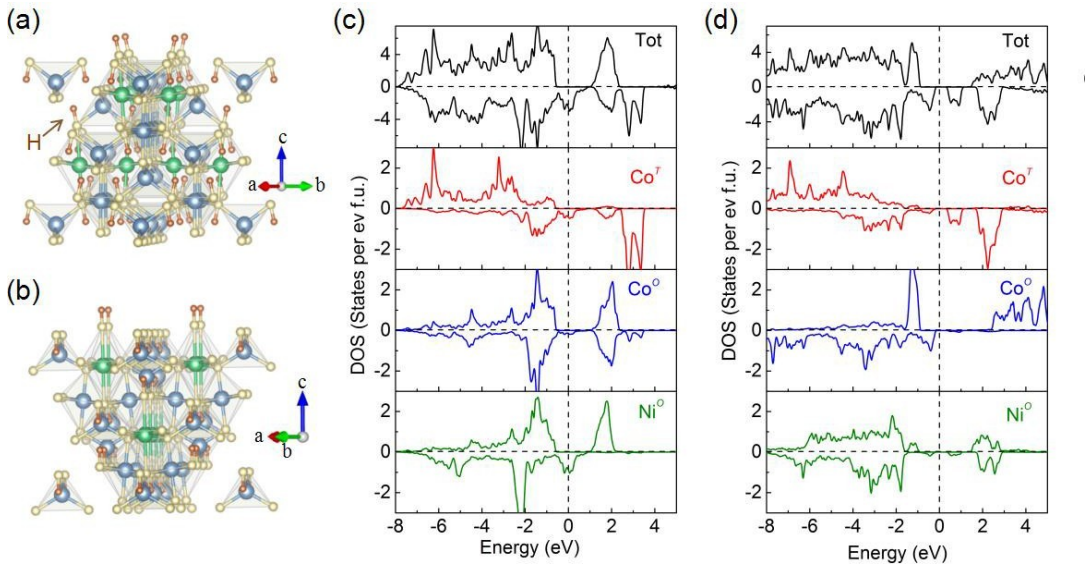

Figure 5. **Calculated lattice structure and density of states (DOS) for pristine and**

protonated samples. a, b) Lattice structure of protonated H2NiCo2O4 from the DFT

calculations viewed along two different crystalline orientations. The proton ions (wine)

tend to bond with the oxygen ions at the Ni (Co)-O octahedra and Co-O tetrahedra,

which leads to the reduced valence states as well as lattice expansion. Calculated

density of states (DOS) for **c**) pristine NCO and **d**) protonated H2NiCo2O4 phases. The

red, blue and olive lines represent the projected DOS for Co ion in tetrahedron (Co^T),

Co ion in octahedron (Co^O) and Ni ion in octahedron (Ni^O) respectively. The vertical

dashed black lines represent the Fermi level.